INTERNATIONAL FIRE DETECTION RESEARCH PROJECT

Field Modeling:
Effects of Flat Beamed Ceilings
on Detector and Sprinkler Response

TECHNICAL REPORT
Year 1

Prepared by

Glenn P. Forney, Ph.D.
Richard W. Bukowski, P.E.
William D. Davis, Ph.D.
Building & Fire Research Laboratory
National Institute of Standards & Technology

NATIONAL
FIRE PROTECTION
RESEARCH FOUNDATION

FIRE RESEARCH

NATIONAL FIRE PROTECTION
RESEARCH FOUNDATION

BATTERYMARCH PARK
QUINCY, MASSACHUSETTS, U.S.A. 02269

Foreword

The International Fire Detection Research Project was initiated in 1990 with the overall aim of improving fire detection and reducing field installation problems. The ultimate goal of this research project is to increase the reliability of placement of heat and smoke sensing systems in spaces with complex ceiling geometries and high ventilation rates.

The first phase of the project resulted in a Literature Review and Technical Analysis, a comprehensive international survey of the literature on fire detection in a variety of subject areas, with suggestions for future research to fill in some of the gaps in the data. A full technical report on the results is available from the Foundation.

The project has progressed to an ambitious four year Research & Development phase. This technical report documents results from the first year's work. Some highlights include:

- The ability to quantify stratification effects in spaces with vertical temperature gradients that exceed the fire plume's temperature.
- Analysis of the conditions produced by smoldering fires with rates of heat release as small as 100 Watts.
- Quantification of the impact of compartment size on the rate at which ceiling pockets between beams or joists fill with hot gases and smoke, relative to sensor locations within the pockets or on the bottoms of beams.

The Research Foundation expresses its gratitude to NIST's Building and Fire Research Laboratory's research team leader, Richard W. Bukowski, and the authors, for their ground-breaking work using sophisticated 3-dimensional field modeling techniques. And the Foundation also wishes to thank Industrial Risk Insurers for their special assistance with the production of this report.

The Foundation and the authors wish to thank the project's sponsors, the Fire Detection Institute and Technical Advisory Committee listed on the next page for their contributions of expertise, and the financial resources required to complete the first of the four years of research. Opinions expressed here are those of the authors. Of course, sponsorship does not necessarily constitute a sponsor's agreement with every statement in this report.

INTERNATIONAL FIRE DETECTION RESEARCH PROJECT

Three Dimensional Field Modeling for Fire Protection

TECHNICAL ADVISORY COMMITTEE

Allied-Signal Aerospace Co.
Automatic Fire Alarm Association
Bellcore
Building Officials & Code Administrators
Canadian Fire Alarm Association
Carmel-by-the-Sea, CA Fire Marshal
Cerberus Technologies
Edwards Systems Technology
Environment One
Electric Power Research Institute
Fire Detection Institute
IEI/Vesda
Industrial Risk Insurers
International Conference of Building Officials
International Fire Code Institute
Liberty Mutual Insurance Company
National Electrical Manufacturers Association
National Institute of Standards & Technology
NFPA Technical Committee on Automatic Sprinklers
North Carolina Department of Insurance
SFPE Educational and Scientific Foundation
Simplex Time Recorder Co.
Southern Building Code Congress, International
System Sensor & Firelite/Notifier
Underwriters Laboratories Inc.
U.S. Fire Administration
U.S. General Services Administration

Contents

List of Figures

List of Tables

Simulating the Effect of Flat Beamed Ceilings on Detector and Sprinkler Response

Glenn P. Forney Richard W. Bukowski William D. Davis

Abstract

This report documents the work performed during the first year of the International Fire Detection Research Project sponsored by the National Fire Protection Research Foundation (NFPRF). The first task was to confirm that fire sensor response can be evaluated using computational data obtained from numerical simulations. A field model was verified for this application by showing that its temperature predictions match experimental results obtained earlier by Heskestad and Delichatsios. The second task consisted of performing a parameter study to show the effect of sensor response under beamed ceilings for various geometries and fire growth rates. One question that is addressed is under what conditions can sensors be located on beams rather than in beam pockets. Time to sensor activation contour plots are presented that address this question. Twenty cases were run for various fire growth rates, beam depths, beam spacings and ceiling heights. These data are summarized and recommendations are made on placing sensors in rooms with beamed ceilings.

1 Introduction

The rapid activation of fire detection and suppression systems in response to a growing fire is one of the important factors required to provide for life safety and property protection. Rapid activation requires that the sensors be located at an optimal distance both beneath the ceiling and radially from the fire. Ceiling obstructions to the movement of heat and smoke such as beams and joists must be taken into account when the system is designed, but little quantitative information is contained in the standards.

Experiments were performed by Heskestad and Delichatsios in the late seventies in order to evaluate the response of fire sensors under flat ceilings[1, 2] and beamed ceilings[3, 4]. Quoting from [3],

> "The major objective of this work was to generate graphical and tabular presentations of the environmental data in both physical forms and "reduced" forms,

the latter allowing extrapolation of the data to arbitrary combination of ceiling heights and fire-growth rates. A second objective was to confirm previously established methods of predicting the response of fire sensors from the environmental data and subsequently to determine optimum spacing of fire sensors under large beamed ceilings."

These goals can also be realized by using numerical simulations to produce the data from which graphical and tabular presentations are derived. This report describes the three step process which was used to accomplish this. First, it was shown that numerical simulations could predict experimental temperature measurements given in [4]. Second, a series of simulations were performed to study the effect of fire growth rates, beam depths, beam spacing and ceiling heights on smoke flow under beamed ceilings. Finally, the results from these simulations were analyzed in order to determine how effective placement of sensors can be influenced by the above room/fire configurations. Ultimately, the goal of this work is to provide a basis for sound recommendations for modifications to the Standard on Automatic Sprinklers (NFPA 13) and the National Fire Alarm Code (NFPA 72).

2 Modeling Assumptions

Release 2.3.2 of Harwell-FLOW3D[5] was used to perform the numerical simulations described in this report. This field model has been previously applied to study the fire at the King's Cross underground station [6]. These numerical results were subsequently verified with 1/3 scale fire experiments[7]. The field model has been successfully applied to two well instrumented full scale room experiments[8]. It was also used to predict the interaction of wind, a fence and a fire near an outdoor fire training facility[9] which was subsequently verified by construction modifications.

2.1 Conservation Equations

The modeling technique used to simulate smoke flow is to divide the region of interest into a collection of small rectangular boxes or control volumes. The conditions in each control volume are initially ambient. Heat is then released in several control volumes over time. The resulting flow or exchange of mass, momentum and energy between control volumes is determined so that these three quantities are conserved. The momentum conservation equations are equivalent to Newton's second law of motion and are sometimes referred to as the *Navier-Stokes* equations. The energy conservation equation is equivalent to the first law of thermodynamics. These fluid flow equations are expressed mathematically as a set of simultaneous, non-linear partial differential equations. After being discretized, the

resulting finite volume[1] equations are solved iteratively using a variant of Newton's method for computing coupled non-linear algebraic equations.

The difficulty of computing these fluid flow equations can be better appreciated by considering the following example. Suppose that each edge of a box is divided into five parts. There are then 125 control volumes. For laminar (*ie* non-turbulent flow) there are 5 unknowns (pressure, temperature, and momentum for each of the three coordinate directions) for each control volume. There are then 625 unknowns to be determined at each stage of the solution process. The full matrix if set up would have 625^2 elements which would require 3,125,000 bytes to represent in double precision. The grid used in the case study has 6555 control volumes and 45885 unknowns (gridded $23 \times 15 \times 19$, 7 unknowns per control volume). Sparse matrix techniques are required to store the matrix[2] and iterative techniques are required to compute the solution.

2.2 Turbulence

The control volume size needs to be consistent with the scale size of the phenomena of interest. Applying this criteria to turbulence would result in problems with many more control volumes than could possibly be solved with today's computers (or computers in the foreseeable future). As a result, turbulence models have been developed to account for the effect of small-scale fluid motion on motion in the larger-scale control volumes. A turbulence model is then a sub-grid model in the sense as used in zone fire modeling. That is, a turbulence model estimates the effect of small scale or sub-grid phenomena on motion in the larger scale.

The first step in constructing a turbulence model is to modify the fluid flow equations by averaging them over both space and time. The unknown pressures, momentums and energies are then interpreted as average rather than instantaneous values. This modified set of fluid flow equations, however, has more unknowns than equations. Turbulence models are then used to to achieve the necessary closure. A model developed in the early seventies is the $k - \epsilon$ model[10]. This model results in two more unknowns per control volume, the turbulent kinetic energy or k and the rate at which this energy dissipates or ϵ. The $k - \epsilon$ family of turbulence models contain several unknown empirical parameters. These parameters are chosen to cause a good fit (usually to minimize the least-square error) between a set of experiments and a corresponding set of modeling results. Each application area potentially requires a different set of parameter values. At the very least the model needs to be run against experiment to verify that reasonable results are obtained. The standard model assumes that turbulence has no preferred direction (is isotropic). In a

[1] The unknowns in finite volume equations are at the center of the control volume while the unknowns in finite difference equations are at the edge or corners.

[2] Only 7 diagonals are non-zero if 3-d rectangular geometries are being modeled

fire plume, temperature induced density variations result in buoyancy forces which cause the plume to rise. The isotropic assumption is violated since these forces occur only in the vertical direction. Frictional forces occurring near solid wall boundaries can cause a similar violation of the turbulence model assumptions. We ran several cases comparing various forms of the $k - \epsilon$ turbulence model and did not find any significant difference in the temperature predictions. We therefore used the simpler form of the $k - \epsilon$ turbulence model which did not involve terms to account for buoyancy.

2.3 Compressibility

The required physical parameters for these equations include fluid density, pressure, specific heat at constant pressure, acceleration of gravity, thermal conductivity and molecular viscosity. It was assumed that the fluid was air and that it was compressible. This assumption may be relaxed in the future, subject to verification, by 1) neglecting the propagation of pressure waves (assuming that the speed of sound is infinite) or 2) assuming that density variations are only important in the momentum equation (Bousinesq approximation). Making either of these assumptions will improve the speed of the model and hence shorten either run times or allow for a more refined grid.

2.4 Heat Transfer

All solid surfaces were assumed to be adiabatic. Clearly heat is transferred from the gas to the walls. This assumption will result in warmer gas temperature predictions than without it since no convective heat transfer occurs between the gas and the walls. For wall materials that are nearly insulating, the wall temperatures will quickly rise to the gas temperature which reduces the heat transfer. The time period over which a parcel of gas is in contact with a wall surface is on the order of seconds[3]. From these two observations we conclude that the adiabatic assumption is reasonable.

Radiation effects were not included in the calculation except that only a fraction of the heat release rate was assumed to contribute to convective heating of the smoke and air. The rest of the heat was considered to be radiated away. This assumption produces the greatest error since 1) the fraction of heat radiated away is unknown and 2) the gas temperatures are very sensitive to fire growth rates. The radiative loss fraction, χ_r, is then a calibration parameter similar to the ones used for the turbulence models discussed above.

[3] scale length of ceiling / fluid velocity = transit time $\approx$ 10 m / 2 m/s = 5 s

2.5 Boundary Specifications

A rectangular, non-uniform grid was used to model each experiment. An upwind differencing scheme was used to model the advection terms. The equations were advanced in time using a fully implicit backward difference procedure.

The grid was set up so that the fire was at the origin (see Figure 1). Six boundary conditions are required, one for each of the six bounding surfaces that define the region begin modeled. The floor and beamed ceiling are assumed to be solid. A no-slip boundary condition was assumed. This means that the velocity both perpendicular and parallel to the boundary are specified to be zero. The two surfaces opposite the fire are constant pressure boundaries. Flows are specified so that velocity gradients are zero at the boundary (*ie.*the flow does not speed up or slow down at the boundary). The two surfaces nearest the fire are specified as symmetric boundaries. Fluid flow is specified to be parallel to the boundary surface so that no flow occurs across it. The two symmetry planes split the experimental region into four regions.

2.6 Fire

In the Factory Mutual (FM) experiments, the fire source consisted of a wooden crib constructed with 15 layers, 14 sticks per layer of clear sugar pine. Each stick had dimensions[4] of 0.0159 m $\times$ 0.0159 m $\times$ 0.762 m (5/8 in $\times$ 5/8 in $\times$ 30 in) Heskestad and Delichatsios used the following procedure in [3] to determine the energy release rate of the fire. Cumulative weight loss was measured for the burning crib for each experiment. This data was then converted to average burning rates using the experimentally determined value of heat of combustion for clear sugar pine of 20.9 MJ/kg (9000 Btu/lb). It was noted in [4] that a plot of the square root of the energy release data versus time was approximately linear. Therefore the burning rates were used to curve fit the expression

$$\sqrt{\dot{Q}(t)} = \sqrt{\alpha}(t - t_0)$$

or equivalently

$$\dot{Q}(t) = \alpha(t - t_0)^2 \, .$$

where $\dot{Q}(t)$ is the heat release rate at time t, α is a proportionality constant and t_0 is the time origin.

Radiation losses from the fire were estimated to be 35 per cent ($\chi_r = 0.35$). Numerical simulations were performed using χ_r values of 0.25, 0.35 and 0.45 . It was found that

[4]For the most part all lengths in the FM work were recorded as a whole number of inches or feet. Distances in this report were converted to the S.I. system of units by using the standard conversion factor of 0.305 m/ft and truncating the result to three significant figures.

$\chi_r = 0.35$ gave the best agreement between the numerical predictions and experiment. The numerical time origin, t_0 was set to zero. The heat release rate used to simulate the FM experiments was then

$$\dot{Q}(t) = \frac{(1-\chi_r)\alpha}{4} t^2$$

where $\chi_r = 0.35$, α is given by Table II on page 13 in [4]. The number 4 arises using a symmetry argument since only one of four quadrants are simulated and it is assumed that the fire contributes equally to each quadrant. The virtual time origins, t_0, found in this table were used to specify the starting time of the experiment for the purpose of comparison.

3 Model Verification

Numerical field modeling can effectively complement laboratory experiments as long as the two approaches give consistent results in a comparable time. The next two sub-sections present results that show that the two approaches are in good agreement. A typical 5 minute simulation using 3105 control volumes took approximately 48 hours of computer time on a Silicon Graphics 4D35 work station. Grids for the parameter study were refined in order to better resolve the ceiling jet near the beams. These simulations, using 6555 control volumes, took approximately 36 hours on an Silicon Graphics R4000 Indigo. This Indigo is approximately 2.5 times faster than the 4D35. For simple grids, it usually takes a few hours to set up a case. Several runs are required to insure that a case is set up correctly. Thus the cumulative time for setting up and running a field model is shorter than the time required to set up and perform a comparable laboratory experiment. Therefore field modeling is a good approach for solving these types of problems.

Six beam configurations were investigated experimentally in [3, 4]. Three configurations consisted of beams with dimensions 0.305 m (1 ft) by 0.152 m (6 in) with 0.61, 1.22 and 1.83 m (2, 4 and 6 ft) on center (OC) spacing. The other three configurations consisted of beams with dimensions 0.61 m (2 ft) by 0.305 m (1 ft) with 1.22, 2.44 and 3.66 m (4, 8 and 12 ft) OC spacing. Each of these six configurations consisted of a suspended beamed ceiling with no walls and a solid floor. The ceiling was moved to keep the distance between the top of the crib and the bottom of the beams at 2.44 m (8 ft). Therefore, the 0.305 (1 ft) beam depth experiments had a ceiling height of 3.05 m (10 ft) while the 0.61 (2 ft) beam depth experiments had a ceiling height of (11 ft). Three experiments were performed for each configuration. An additional three experiments were performed with draft curtains in addition to the beams.

A short beam spaced experiment, experiment 4, and a medium beam spaced experiment, experiment 16, were chosen for the comparisons in this report. The large beam spaced experiments, 19, 20 and 21, required more grids to simulate two channels than the short

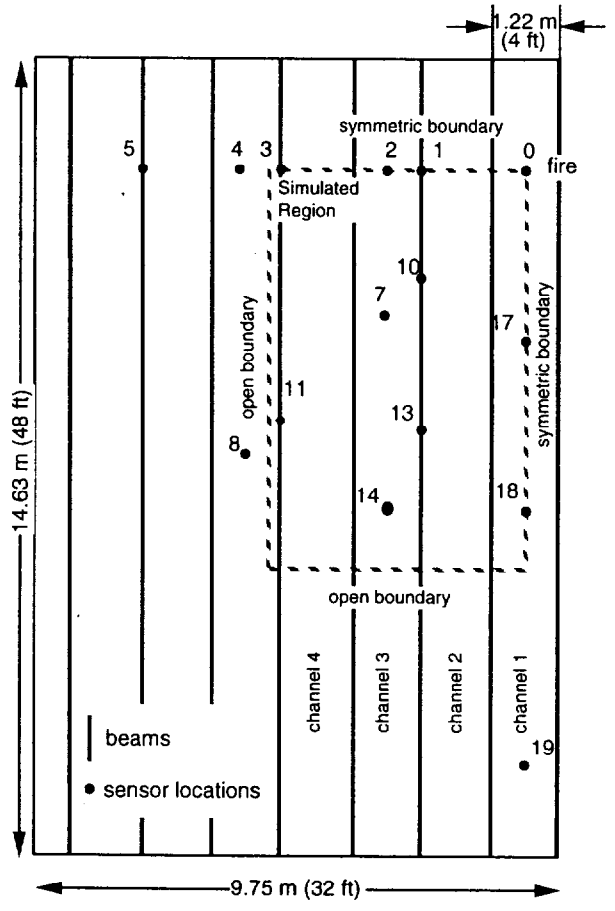

Figure 1: Physical Configuration for Experiment 4

and medium case. Experiment 4 consisted of ceiling beams spaced 1.22 m (4 ft) apart with a depth of 0.305 m (1 ft). Experiment 16 consisted of ceiling beams spaced 2.44 m (8 ft) apart with a depth of 0.61 m (2 ft). Numerical results predicted by the field model are shown to be in substantial agreement for these two experiments.

3.1 1.22 m (4 ft) OC Spaced Experiment

Figure 1 shows a schematic of the top view for the setup for experiment 4. This figure corresponds to Figure 1b in [4]. The numbers denote temperature sensor locations. These sensors are located 0.152 m (6 in) below the ceiling. The ceiling height is 3.05 m (10 ft). The x and y locations are detailed in Table 1. The distances are measured with respect to

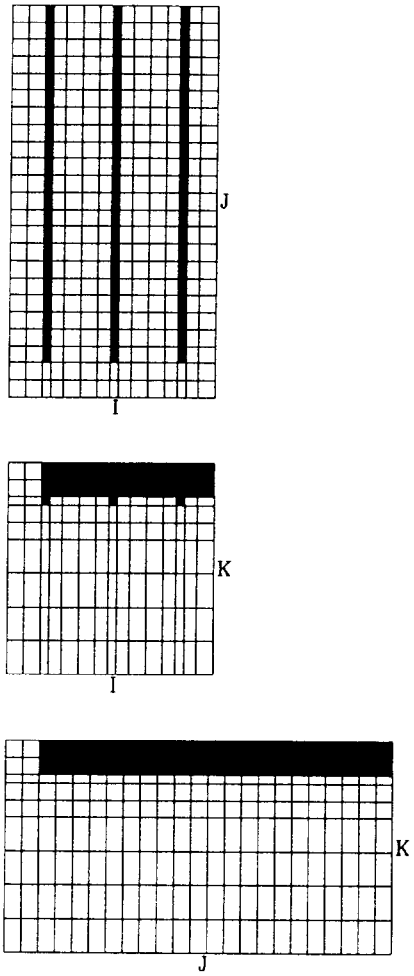

Figure 2: Grid Used to Simulate Experiment 4

the fire. The fire source, a wood crib, was located at position 0 as a point source of energy. The grid used to simulate this experiment is shown in Figure 2.

The portion of the experiment simulated using the field model is outlined with the small interior rectangle in Figure 1. The simulated region includes four flow channels. A channel refers to the space near the ceiling between adjacent beams. The beams tend to isolate or channel the smoke flow. Therefore, the temperature tends to drop more rapidly (towards ambient) across channels than within a channel. Because of this, four channels are sufficient to simulate the main features of the experiment. The vertical grid dimensions near the floor are 0.61 m (2 ft) while grids near the ceiling have a vertical dimension of 0.305 m (1 ft). The horizontal grid dimensions are for the most part 0.305 $\times$ 0.305 m (1 ft $\times$ 1 ft). The grids are smaller near the beams to better resolve the flow and to simulate the correct beam

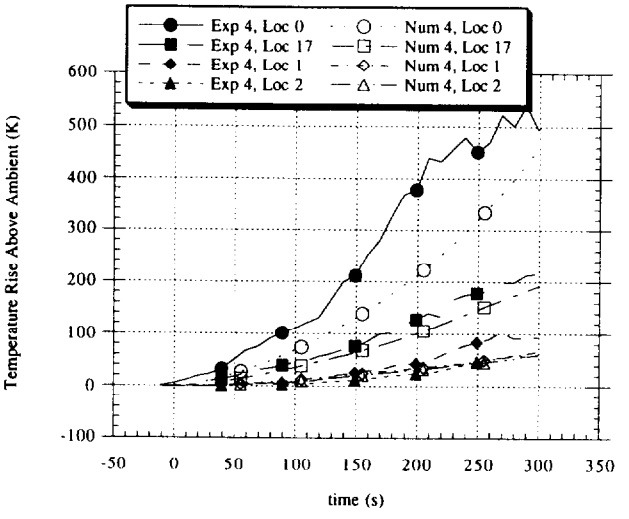

Figure 3: Comparison of Numerical and Experimental Temperatures at Sensor Locations 0, 17, 1 and 2 for Experiment 4

spacing.

Figure 3 shows temperature comparisons for location 0 (above the fire), location 17 (in first channel), location 1 (under the beam separating the second and third channel) and location 2 (in the third channel). Temperature comparisons for other locations (18, 10, 13, 7 and 14) are similar to those shown in Figure 3. Temperature comparisons were made for all locations within the shaded rectangle except for locations 3 and 11. These locations are under the beam in the fourth channel. The experimentally measured temperature rises were approximately 10 °C (18 °F) at 300 seconds.

The field model calculates the temperatures at the center of each grid cell. The temperature at the instrument locations were calculated by linearly interpolating this data using the B3INK/B3VAL software [11] which implements tensor product B-spline interpolation algorithms [12, 13].

The agreement between numerical and experimental temperature measurement directly over the fire is not good. This discrepancy is likely caused by radiation heat transfer not accounted for in the experimental temperature measurement. The flame height was estimated to be 2.8 m (9.2 ft) using Heskestad's flame height correlation[14], $L = -1.02 + 0.235\dot{Q}^{2/5}$ and assuming that $\dot{Q} = 1000kW$. This is consistent with Figure 10 on page 25 of reference [4] which shows a photograph of a 0.61 m (2 ft) beam depth experiment 6 minutes into a simulation. Noting that the flame tip reaches the bottom of the beams, it can be inferred that the flame height is 2.74 m (9 ft).

Table 1: Instrument Locations Used in the Experiment 4 Comparison

Instrument Location	X (m)	Y (m)
0	0.00	0.00
1	1.83	0.00
2	2.44	0.00
7	2.44	2.44
10	1.83	1.83
13	1.83	4.42
14	2.44	5.88
17	0.00	3.05
18	0.00	6.10

Temperature comparisons at other locations, are good. The field model successfully predicts quantitatively the temperature rise with time and the temperature drop off that occurs going from the first channel containing the fire to the third channel. The experimental data used for the comparison was obtained from [3].

Figures 4 and 5 show how the hot gasses generated by the fire plume are channeled by the beams. The fire in Figure 5 is located in the upper right corner. The shaded contours represent the temperature rise in °C above ambient. The contours in Figure 4 lie in a vertical plane perpendicular to the beams 3.05 m (10 ft) from the fire. The contours in Figure 5 lie in a plane parallel to the floor 0.152 m (6 in) below the ceiling. Similar contour plots with shorter beam depths show, as expected, smoke flow that is less channeled.

3.2 2.44 m (8 ft) OC Spaced Experiment

Figure 6, similar to Figure 1, shows a schematic of the top view of the experimental configuration for experiment 16. The essential difference between these two figures is that the beams are spaced 2.44 m (8 ft) apart rather than 1.22 (4 ft) apart. Due to the wider spacing, the temperature comparisons are made in adjacent channels rather than every third channel. Again, the numbers denote the temperature sensor locations. The sensors are located 0.152 m (6 in) below the ceiling (or beam) and the fire source is located at position 0. The ceiling height is 3.36 m (11 ft). The thick solid line denotes the beams and the dashed inner rectangle indicates the portion of the physical experiment that was simulated numerically. Temperature comparisons made at location 0 (over the fire), 17 (in the first channel near the fire) and 1 (in the second channel) are shown in Figure 7. Data for the comparison was obtained from [3]. Comparisons were also made at locations 18, 7, 14 and

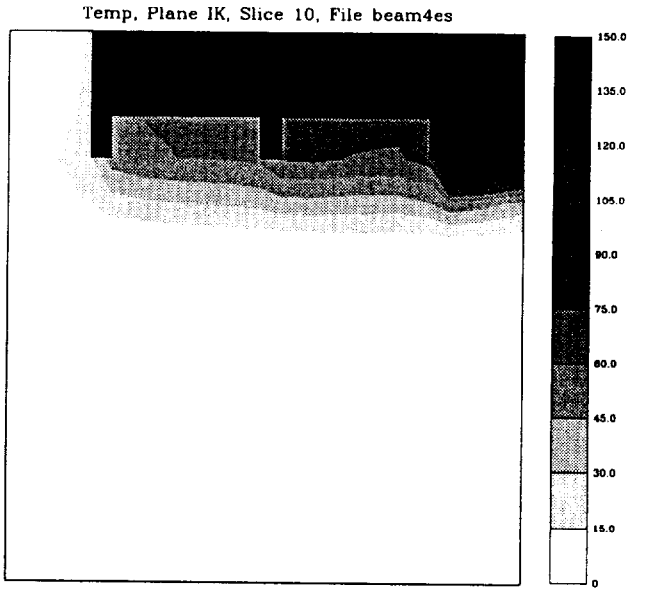

Figure 4: Shaded Temperature Rise Contours (° C) for Experiment 4 in a Vertical Plane Perpendicular to the Beams 3.05 m (10 ft) from the Fire at 300 seconds

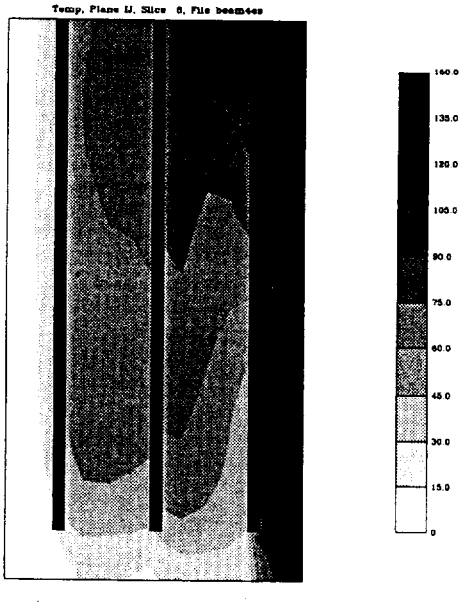

Figure 5: Shaded Temperature Rise Contours (° C) for Experiment 4 in a Plane Parallel and 0.152 m (6 in) Below the Ceiling at 300 seconds

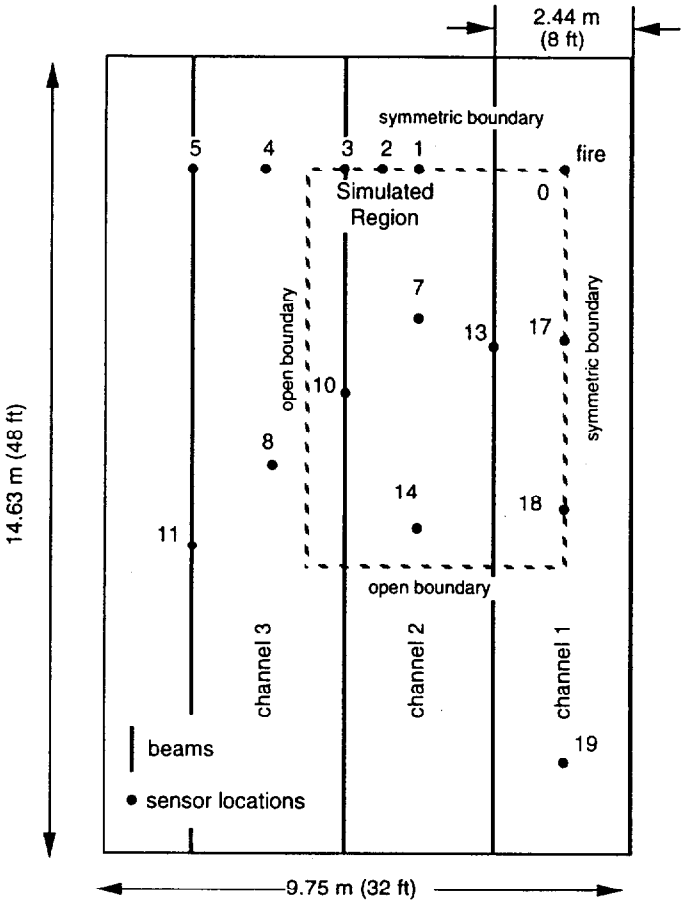

Figure 6: Physical Configuration for Experiment 16

Table 2: Instrument Locations Used in the Experiment 16 Comparison

Instrument Location	X (m)	Y (m)
0	0.00	0.00
1	1.83	0.00
7	1.83	2.44
14	1.83	5.88
17	0.00	3.05
18	0.00	6.10

2 with comparable results. The experimentally measured temperature rise at location 3 and 10 was only 7.2 °C (13.0 °F), 5.0 °C (9.0 °F) respectively. The physical locations of these instruments are recorded in Table 2. As seen in the plot, the numerical and experimental temperature measurements compare quite well for each sensor location. The comparison over the fire is better in this experiment than in the 0.305 (1 ft) beam depth experiment since there is a 0.61 m (2 ft) gap between the flame tip and the sensor instead of a 0.305 m (1 ft) gap. Again, the field model predicts quantitatively both the temperature rise with time and the temperature fall off that occurs in adjacent channels including the sensors directly over the fire.

Figure 8 shows shaded temperature contours 0.167 m (6 in) below the ceiling. The fire is located in the upper right corner of Figure 9. The smoke flow is contained within the beam channels more in this experiment than in Experiment 4 since the beams depths are 0.610 m (2 ft) instead of 0.305 m (1 ft). The contours in Figure 8 lie in a vertical plane perpendicular to the beams 3.05 m (10 ft) from the fire. The contours in Figure 9 lie in a plane parallel to the floor 0.152 m (6 in) below the ceiling. A comparison of the contour plots in Figures 8 and 4 shows the effect of the deeper beams and wider channels. The temperature drop off between adjacent channels is greater for experiment 16 (compare second channels in Figure 4 and Figure 8).

4 Case Study

4.1 Scope

The next step in this work was to perform a series of numerical experiments for configurations not given in [3] in order to study the effects of beam depths, beam spacing, ceiling heights and fire growth rates on the distribution of heat and smoke near the ceiling and their

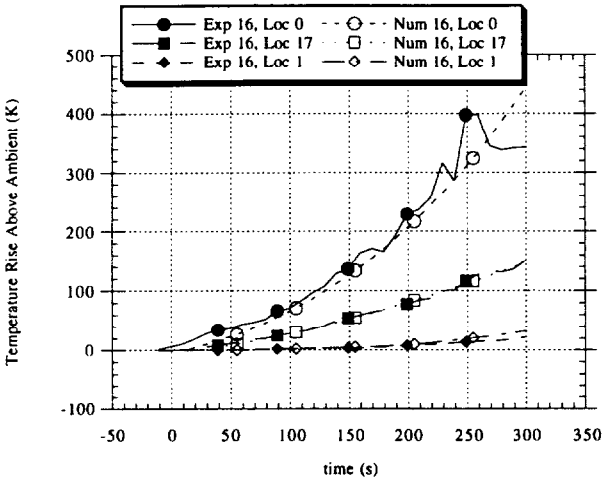

Figure 7: Comparison of Numerical and Experimental Temperatures at Sensor Locations 0, 17 and 1 for Experiment 16

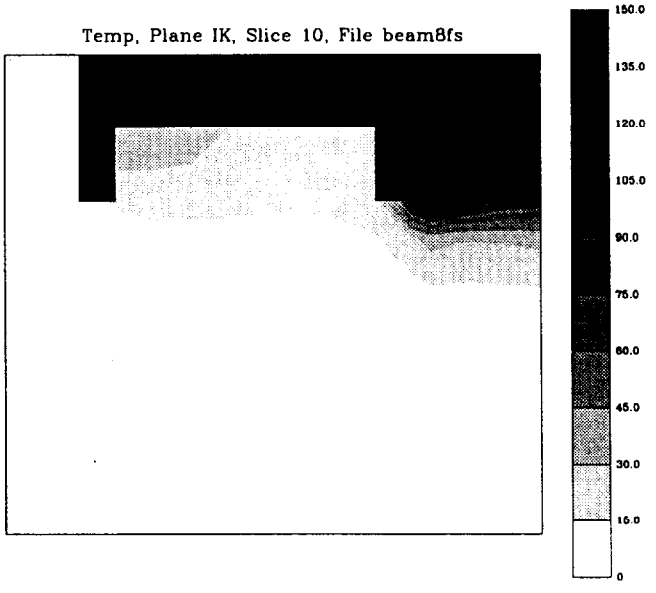

Figure 8: Shaded Temperature Rise Contours ($°C$) for Experiment 16 in a Vertical Plane Perpendicular to the Beams 3.05 m (10 ft) from the Fire at 300 seconds

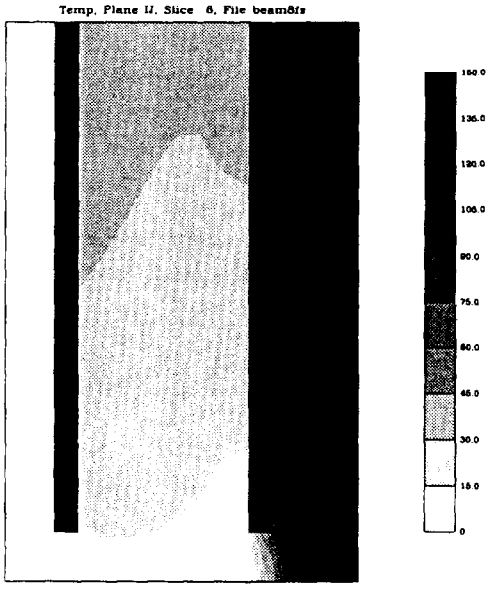

Figure 9: Shaded Temperature Rise Contours (° C) for Experiment 16 in a Plane Parallel and 0.152 m (6 in) Below the Ceiling at 300 seconds

effect on sensor activation. Five series of numerical simulations were performed. The first four series varied one parameter while leaving the other parameters fixed. The fifth series consisted of several cases modeling enclosed spaces. The base case, similar to experiments 4, 5 and 6 in [3], consisted of a 't^2' fire which reached 1.055 MW (1000. Btu/s) in 275 seconds, a ceiling height of 3.36 m (11 ft) and beam depths of 0.305 (1 ft). Figure 10 shows the grid for the IJ, IK and JK plane where the I axis is horizontal and perpendicular to the beams, the J axis is horizontal and parallel to the beams and the K axis is vertical. The vertical dimension of the grid near the ceiling is 0.076 m (3 in) in order to resolve better flows around the beams. Vertical grid dimensions near the floor were 0.305 m . Horizontal spacing parallel to the beams is 0.305 m. Horizontal spacing perpendicular to the beams were chosen to insure the proper on center beam spacing which ranged from 1.22 m (4 ft) to 2.44 m (8 ft).

The NFPA 72E[15] standard defines *fire size* in terms of how long it takes a 't^2' or quadratic fire to reach 1.055 MW (1000 Btu/s)[5]. If

$$q_{fire} = 1.055(t/t_{size})^2$$

is the energy release rate of a fire then reference [15] defines t_{size} for a slow fire to satisfy $t_{size} > 400$, for a medium fire, $150 < t_{size} < 400$ and a for a fast fire to be $t_{size} < 150$. Figure 11 presents a plot of a slow, medium and fast t^2 fire.

[5]While NFPA 72E refers to this as fire size it is more correctly referred to as a fire growth rate.

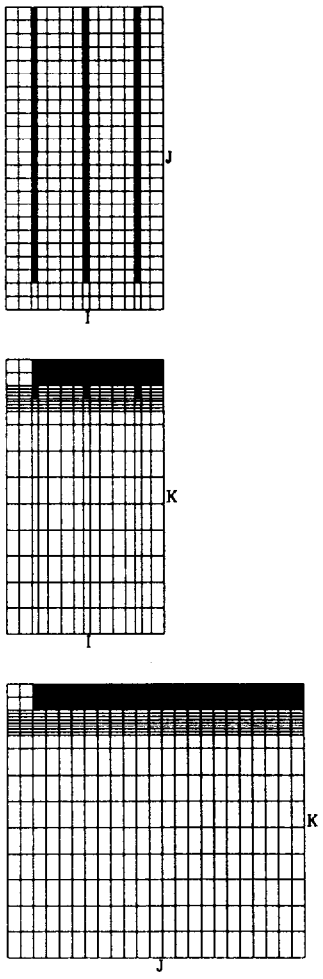

Figure 10: Grid used for the simulation of the base case; medium fire, 3.35 m (11 ft) ceiling, 1.22 m (4 ft) OC beam spacing, 0.305 m (1 ft) beam depth. Note that the cell sizes are smaller in the regions of most interest near the ceiling and obstructions.

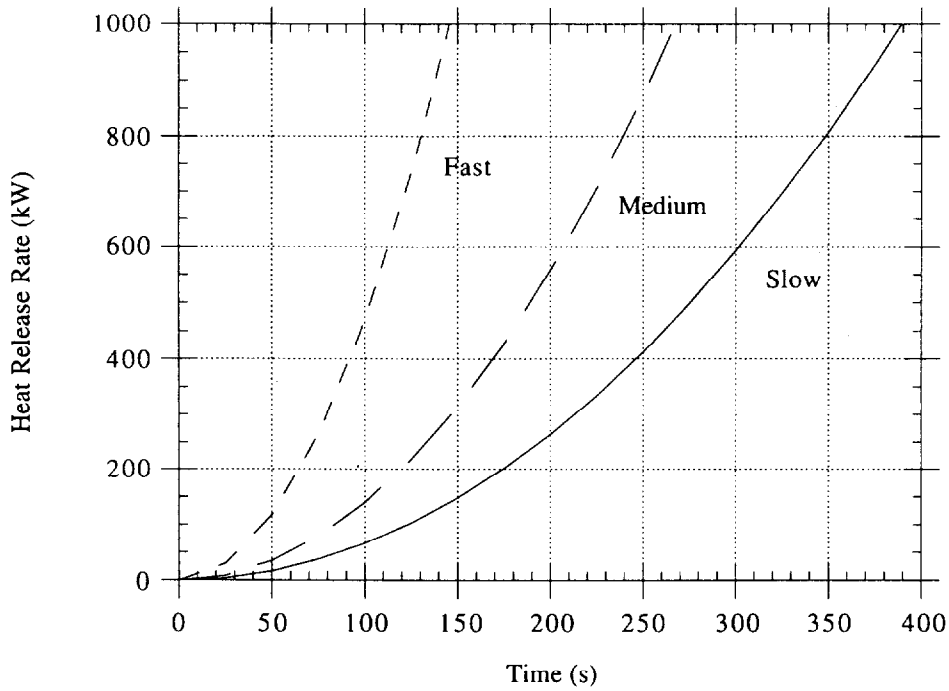

Figure 11: Plot of slow, medium and fast fires versus time

Three cases were run varying the growth rate of the fire. The fire growth rates were slow, medium and fast where $t_{size} = 400$ for the slow fire, $t_{size} = 275$ for the medium fire and $t_{size} = 150$ for the fast fire. The ceiling height, beam depths and center to center beam spacings for these three cases were 3.35 m (11 ft), 0.305 m (12 in) and 1.22 m (4 ft) respectively.

Five cases were run varying the on center spacing between the beams. The spacings were 1.22 m (4 ft), 1.52 m (5 ft), 1.83 m (6 ft), 2.13 m (7 ft) and 2.44 m (8 ft). The fire size, ceiling height and beam depths for these five cases were medium, 3.35 m (11 ft) and 0.305 m (12 in) respectively.

Five cases were run with varying the beam depths. The depths consisted of 0.0 m (0 in), 0.10 m (4 in), 0.20 m (8 in), 0.305 m (1 ft) and 0.61 m (24. in). The fire size, ceiling height, and center to center beam spacings for these five cases were medium, 3.35 m (11 ft), and 1.22 m (4 ft) respectively.

Six cases were run varying the ceiling height. The heights were 3.35 m (11 ft), 4.57 m (15 ft), 5.79 m (19 ft), 6.71 m (22 ft), 7.62 m (25 ft) and 8.53 m (28 ft). The fire size, beam depths and center to center beam spacings for these three cases were medium, 0.305 m (12 in) and 1.22 m (4 ft) respectively.

Three cases were run varying the room area for a case with solid walls (rather than open walls) on all sides. A description of these cases is summarized in Table 3.

Table 3: Description of Numerical Experiments Performed in Case Study

Cases	fire growth rate	beam depth	beam spacing	ceiling height
F1	slow	.305 m (1 ft)	1.22 m (4 ft)	3.35 m (11 ft)
F2	medium	.305 m (1 ft)	1.22 m (4 ft)	3.35 m (11 ft)
F3	fast	.305 m (1 ft)	1.22 m (4 ft)	3.35 m (11 ft)
W4	medium	.305 m (1 ft)	1.22 m (4 ft)	3.35 m (11 ft)
W5	medium	.305 m (1 ft)	1.52 m (5 ft)	3.35 m (11 ft)
W6	medium	.305 m (1 ft)	1.83 m (6 ft)	3.35 m (11 ft)
W7	medium	.305 m (1 ft)	2.13 m (7 ft)	3.35 m (11 ft)
W8	medium	.305 m (1 ft)	2.44 m (8 ft)	3.35 m (11 ft)
B0	medium	0.00 m (0 in)	1.22 m (4 ft)	3.35 m (11 ft)
B4	medium	0.10 m (4 in)	1.22 m (4 ft)	3.35 m (11 ft)
B8	medium	0.20 m (8 in)	1.22 m (4 ft)	3.35 m (11 ft)
B12	medium	0.305 m (1 ft)	1.22 m (4 ft)	3.35 m (11 ft)
B24	medium	0.610 m (2 ft)	1.22 m (4 ft)	3.35 m (11 ft)
H12	medium	.305 m (1 ft)	1.22 m (4 ft)	3.35 m (11 ft)
H15	medium	.305 m (1 ft)	1.22 m (4 ft)	4.57 m (15 ft)
H19	medium	.305 m (1 ft)	1.22 m (4 ft)	5.79 m (19 ft)
H22	medium	.305 m (1 ft)	1.22 m (4 ft)	6.71 m (22 ft)
H25	medium	.305 m (1 ft)	1.22 m (4 ft)	7.62 m (25 ft)
H28	medium	.305 m (1 ft)	1.22 m (4 ft)	8.53 m (28 ft)

4.2 Data Reduction

The field model uses finite-volume equations to represent the fluid flow equations. The solution variables generated by the field model represent values located at the center of a control volume rather than at a grid edge as in finite difference equations. The solution variables must be interpolated onto the grid (or the grid onto the solution variable locations) in order to produce consistent contour plots. This is done by defining the interpolated solution variable at a grid edge to be the average of control volume solution values at all surrounding control volumes. Control volumes which are solid are not included in the averaging process.

Four types of data are then recovered from the field model at each control volume: gas temperature, time at which the gas temperature[6] reaches a given temperature T_{crit}, sensor

[6]The activation time of a smoke detector is estimated using the gas temperature.

temperature data and time at which the sensor activates at a temperature[7] T_{crit}.

The field model was modified to dump the velocity field and temperature scalar field every 5 seconds throughout the 300 second simulations. Temperature contour plots are produced at any time by linearly interpolating temperature data at times in the dump file that bracket the desired time. Activation times for gas temperature devices are calculated by simply noting the *first* time the gas temperature reaches the temperature T_{crit}. For smoke detectors, T_{crit} is taken to be 13 $^{\circ}C$ above ambient. For heat detectors, T_{crit} is taken to be 57.2 $^{\circ}C$ (135 $^{\circ}$ F). The temperature of the sensing element such as found in heat detectors and sprinklers is estimated using the differential equation developed in [16]

$$\begin{aligned} \frac{dT_L}{dt} &= \frac{\sqrt{S(t)}}{\text{RTI}}\left(T_g(t) - T_L(t)\right), \\ T_L(0) &= T_g(0) \end{aligned} \tag{1}$$

where T_L, T_g are the link and gas temperatures in $^{\circ}C$, S is the flow speed of the gas and RTI is a measure of the sensor's sensitivity to temperature change (a thermal inertia). The RTI of sprinkler heads is measured in a standard apparatus[16] for use in system design and activation prediction. Sprinkler head (activation) performance is classified by RTI value. For heat detectors space rating has a similar use and a correlation between space rating and RTI is made in NFPA 72E. This model (equation (1)) assumes that forced convection is the dominant mode of heat transfer. Heat loss due to radiation and conduction are assumed to be small.

Equation (1) is solved for each control volume using the implicit trapezoidal rule. The algorithm is discussed in Appendix A. As this equation is being solved, the time at which the sensor activates is also recorded. These contours, gas temperature activation times and link temperature activation times based on RTI values of 50, 100, 300 are used to determine the effect of sensor placement on activation time.

From examining these contours, several observations can be made which are discussed in the next section.

4.3 Observations and Analysis

Many of the following observations are obvious at least in hindsight but are noted because of the impact they have on sensor siting strategies and related codes.

Observation 1 Beams trap flow. When beams are sufficiently deep no flow gets into adjacent channels. This can result in earlier sensor activation times under beamed ceilings than under smooth ceilings provided that a sensor is located in every channel.

[7] A heat detector, sprinkler link or any sensor with thermal inertia requires a separate model (a simple example of which is given in equation (1)) to calculate the temperature of the sensor

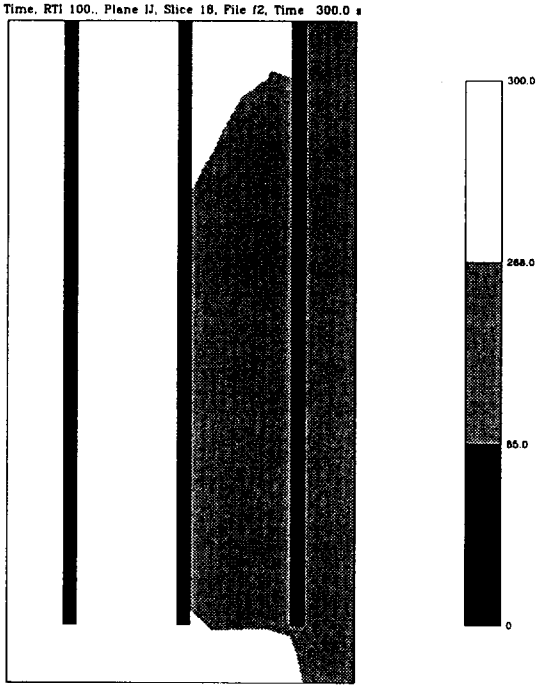

Figure 12: Activation time contours for heat detectors with RTI=100 for the standard case in a horizontal plane 3 inches below the ceiling

Observation 2 A related observation is that beams cause flow near the ceiling to slow down and as a result, temperatures are warmer near the ceiling for beam cases than for non-beam cases. Figure 19 shows a cross-section near the ceiling for several cases with different beam depths. Note that the activation region for the 0.10 m (4 in) and 0.20 m (8 in) beam depth cases is larger than the activation region for the smooth ceiling.

Observation 3 Due to the dependence on $\sqrt{\text{flow velocity}}$, heat detectors can be adversely affected by the reduced ceiling jet velocity as can be seen in Figure 12. The region at the top of the plot (near the fire) in the second channel in Figure 12, which shows activation time, is white because the flow speed is slow as can be seen in Figure 13 (less then 0.5 m/s). Plates 1 through 9 show velocity contours in a plane just below the ceiling, in a plane just below the beams for various beam depth cases. Plate 10 shows velocity contours in a plane perpendicular to the floor and the beams.

Observation 4 The activation time[8] of sensitive sensors (smoke detectors or RTI=50 heat detectors) is independent of fire growth rate. For smoke detectors in Figure 15 and heat detectors (RTI=50) in Figure 16 the response surface for when a sensor activates by the time the fire has reached 1.0 MW are essentially the same. For heat detectors with RTI=100

[8]time normalized to when a fire reaches 1 MW

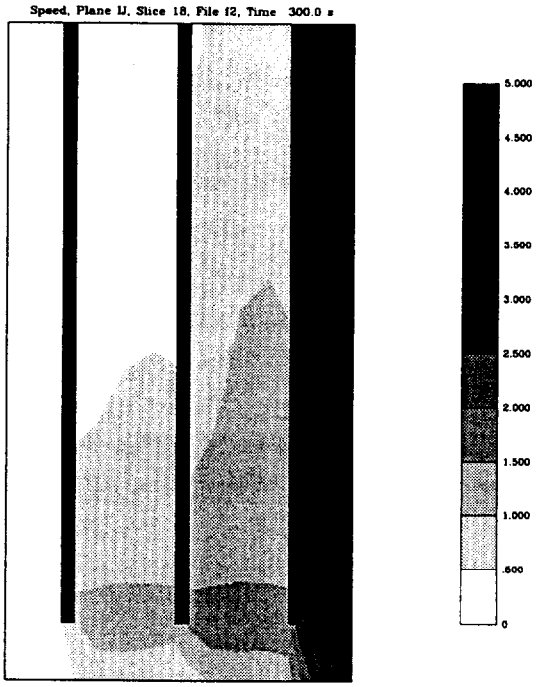

Figure 13: Shaded speed contours for the standard case in a horizontal plane 3 inches below the ceiling

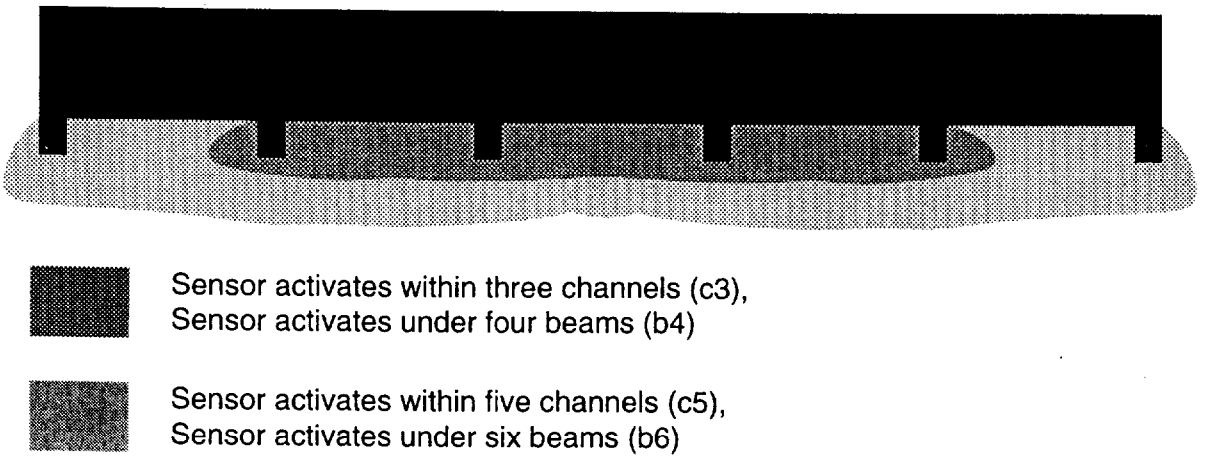

Figure 14: Example of shaded contour plot that includes both sides of the symmetry plane

or RTI=300, the activation response is different between the three fire growth rates f1, f2 and f3 as seen in Figures 17 and 18.

Observation 5 Conditions in beam channels may be equivalent[9] to conditions under beams. Figures 15 to 30 show response volumes for smoke and heat detectors for various beam depths, on center beam spacings, ceiling heights and fire sizes. The surface of the response volumes represent a region where the sensor behaves (*ie* activates in the same time) in the same way. Note that the contour plots are symmetric. It is presumed that the two beams and one channel to the right of the symmetry plane will also activate a sensor. The results of all of the parametric variations on sensor spacing are summarized in Table 4. An entry in this table is determined by examining the corresponding contour plot. If the contour plot shows that a sensor has activated below 2 beams and within 2 channels then the corresponding table entry will be b4/c3. The notation bi or cj means put a sensor under every i'th beam or in every j'th channel.

As an example, examine the contour plot in Figure 14. This figure is the same as the third contour in Figure 19 except that the symmetric portion is included. The dark grey contours are in the middle three channels and under the middle four beams. Therefore the entry under case B8, 100 kW should be b4/c3. The b*i*/c*j* can be obtained for each contour plot by reflecting the plot about the plane of symmetry (the right edge of the figure) in the same way that Figure 14 was generated.

[9] in the sense that a sensor will activate in the same time

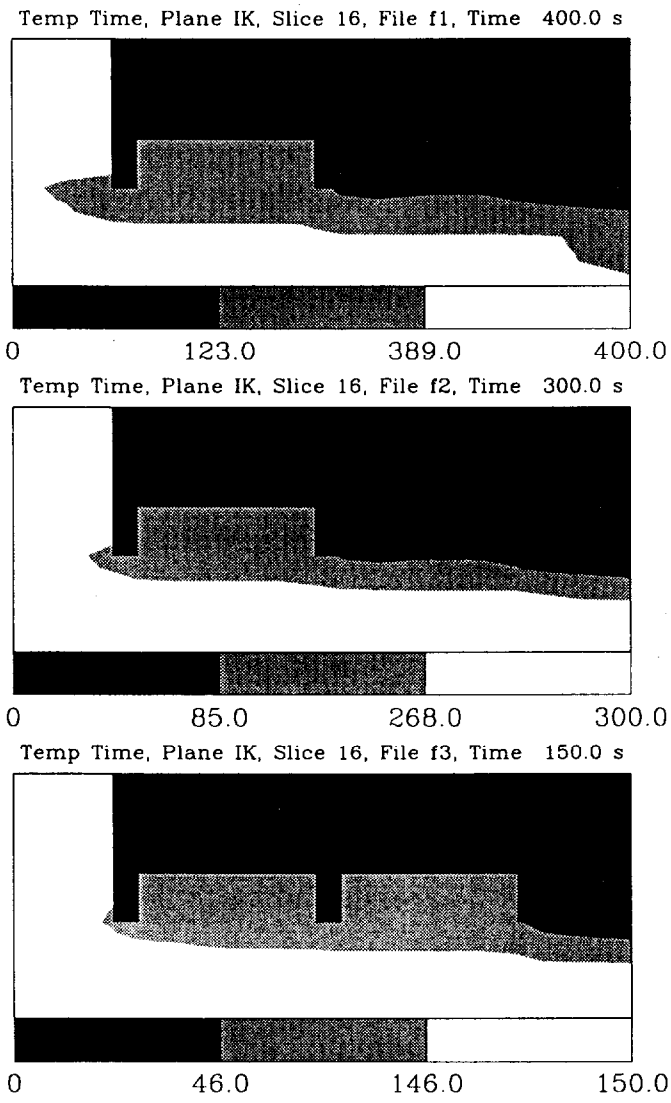

Figure 15: Shaded contour plot of smoke detector response volumes for various fire sizes: slow (denoted f1, reaches 1.0 MW in 389 seconds), medium (denoted f2, reaches 1.0 MW in 268 seconds), fast (denoted f3, reaches 1.0 MW in 146 seconds)with 0.305 m (12 in) beam depth, 3.35 m (11 ft) ceiling height and 1.22 m (4 ft) beam spacing. Dark and light grey denotes where a sensor activates before the fire reaches 100 kW and 1.0 MW respectively. White denotes where the sensor would not activate. Activation criteria: when the gas temperature rises $13°C$ above ambient.

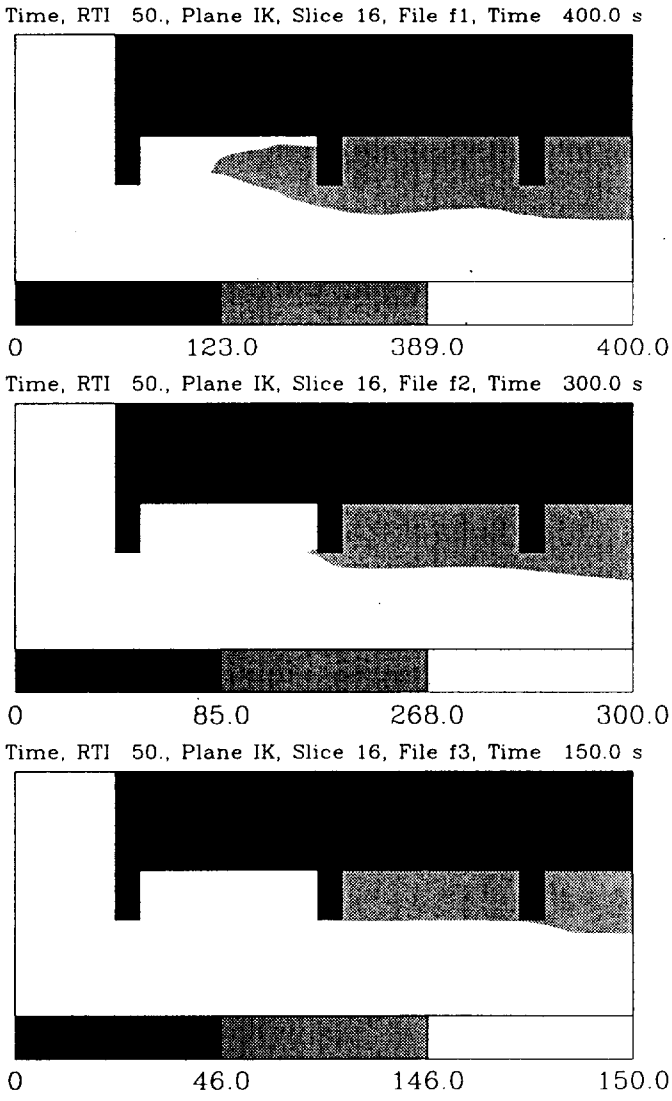

Figure 16: Shaded contour plot of heat detector (RTI = 50) response volumes for various fire sizes: slow (denoted f1, reaches 1.0 MW in 389 seconds), medium (denoted f2, reaches 1.0 MW in 268 seconds), fast (denoted f3, reaches 1.0 MW in 146 seconds)with 0.305 m (12 in) beam depth, 3.35 m (11 ft) ceiling height and 1.22 m (4 ft) beam spacing. Dark and light grey denotes where a sensor activates before the fire reaches 100 kW and 1.0 MW respectively. White denotes where the sensor would not activate. Activation criteria: when the link temperature rises to $57°C$ ($135°F$).

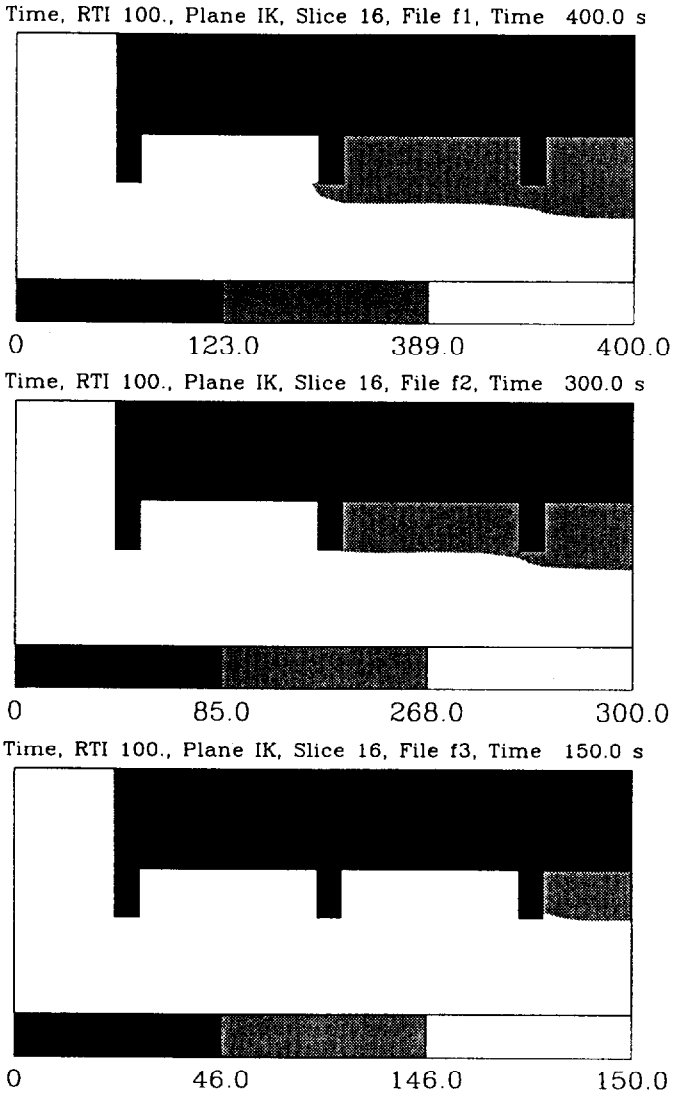

Figure 17: Shaded contour plot of heat detector (RTI = 100) response volumes for various fire sizes: slow (denoted f1, reaches 1.0 MW in 389 seconds), medium (denoted f2, reaches 1.0 MW in 268 seconds), fast (denoted f3, reaches 1.0 MW in 146 seconds)with 0.305 m (12 in) beam depth, 3.35 m (11 ft) ceiling height and 1.22 m (4 ft) beam spacing. Dark and light grey denotes where a sensor activates before the fire reaches 100 kW and 1.0 MW respectively. White denotes where the sensor would not activate. Activation criteria: when the link temperature rises to $57°C$ ($135°F$).

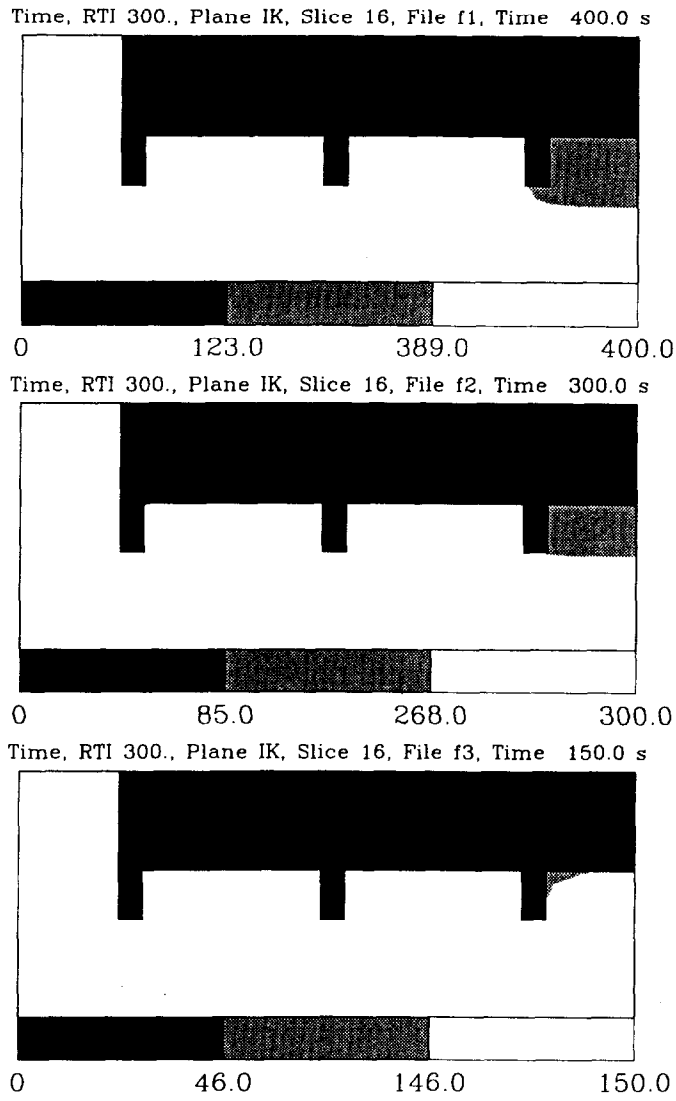

Figure 18: Shaded contour plot of heat detector (RTI = 300) response volumes for various fire sizes: slow (denoted f1, reaches 1.0 MW in 389 seconds), medium (denoted f2, reaches 1.0 MW in 268 seconds), fast (denoted f3, reaches 1.0 MW in 146 seconds)with 0.305 m (12 in) beam depth, 3.35 m (11 ft) ceiling height and 1.22 m (4 ft) beam spacing. Dark and light grey denotes where a sensor activates before the fire reaches 100 kW and 1.0 MW respectively. White denotes where the sensor would not activate. Activation criteria: when the link temperature rises to $57°C$ ($135°F$).

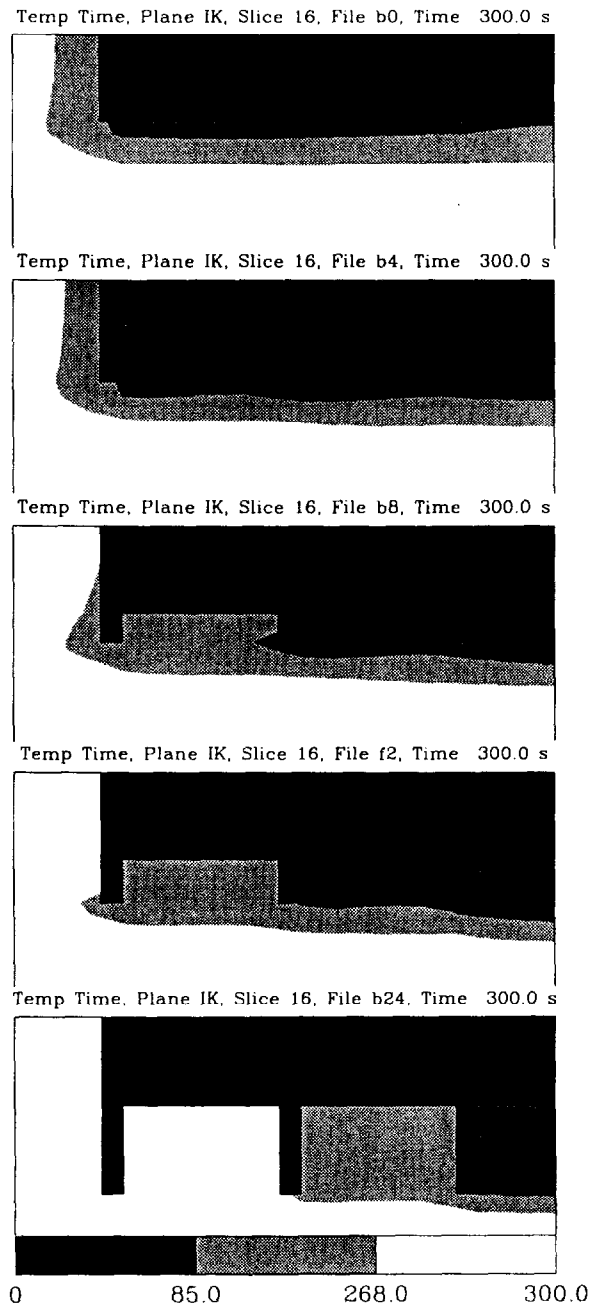

Figure 19: Shaded contour plot of smoke detector response volumes for various beam depths: 0.0 m (0 in), 0.10 m (4 in), 0.20 m (8 in), 0.30 m (12 in), 0.61 m (24 in)with 3.35 m (11 ft) ceiling height, 1.22 m (4 ft) beam spacingand medium fire. Dark and light grey denotes where a sensor activates before the fire reaches 100 kW and 1.0 MW respectively. White denotes where the sensor would not activate. Activation criteria: when the gas temperature rises $13°C$ above ambient.

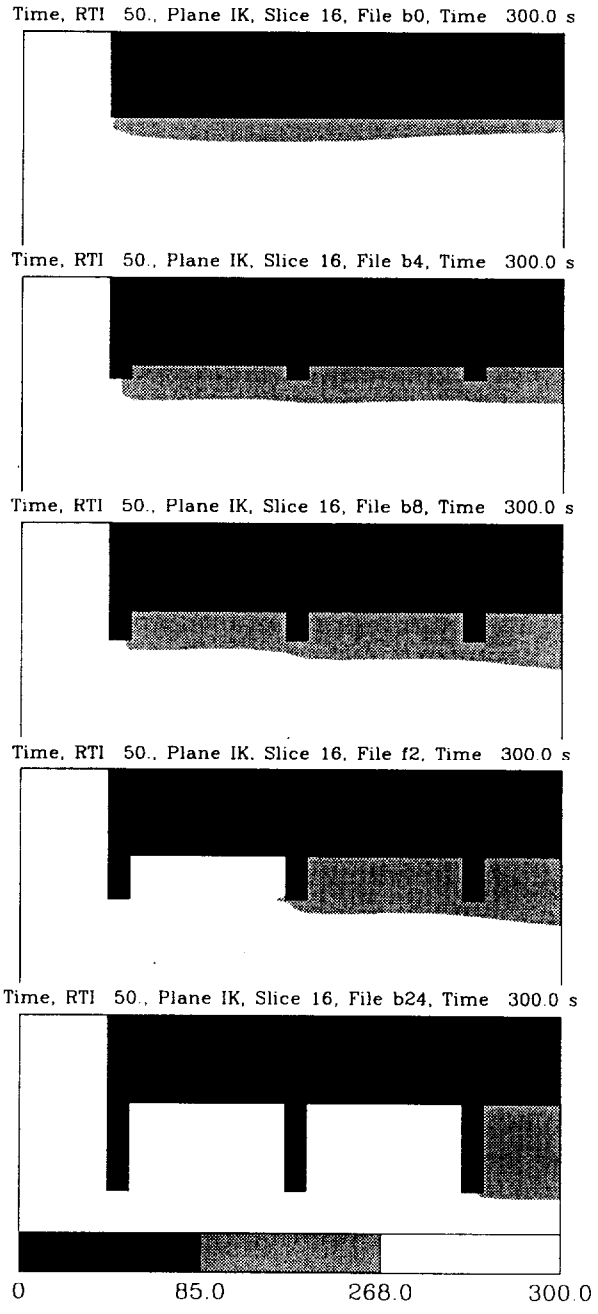

Figure 20: Shaded contour plot of heat detector (RTI = 50) response volumes for various beam depths: 0.0 m (0 in), 0.10 m (4 in), 0.20 m (8 in), 0.30 m (12 in), 0.61 m (24 in)with 3.35 m (11 ft) ceiling height, 1.22 m (4 ft) beam spacingand medium fire. Dark and light grey denotes where a sensor activates before the fire reaches 100 kW and 1.0 MW respectively. White denotes where the sensor would not activate. Activation criteria: when the link temperature rises to $57°C$ ($135°F$).

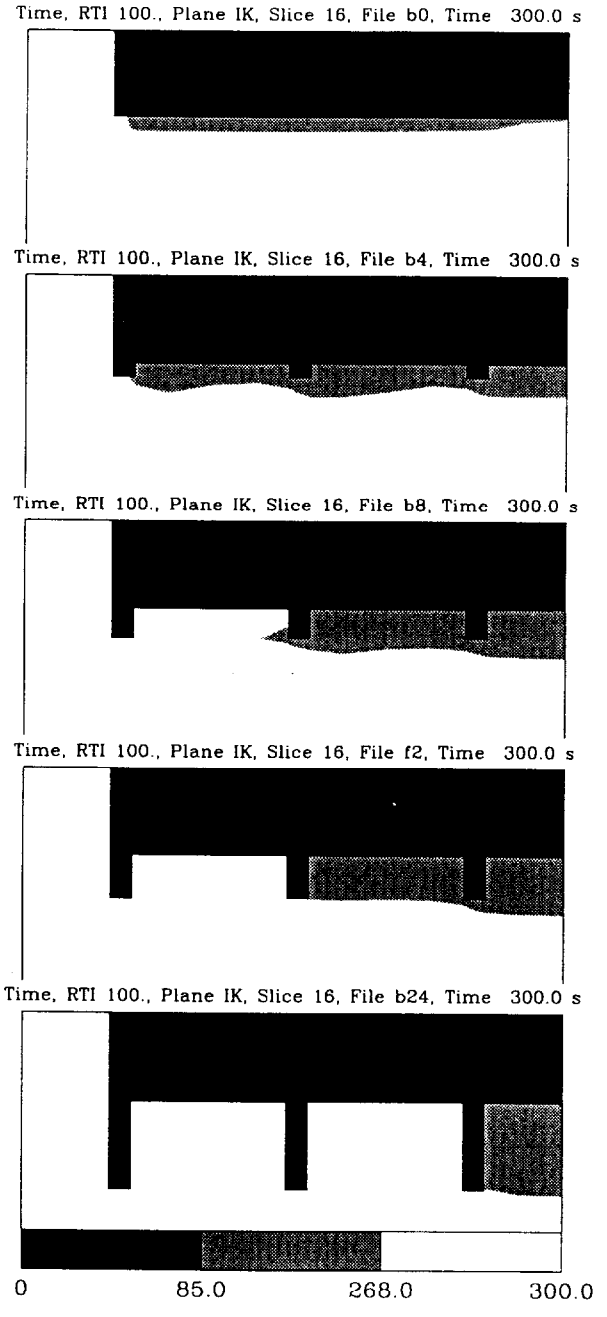

Figure 21: Shaded contour plot of heat detector (RTI = 100) response volumes for various beam depths: 0.0 m (0 in), 0.10 m (4 in), 0.20 m (8 in), 0.30 m (12 in), 0.61 m (24 in)with 3.35 m (11 ft) ceiling height, 1.22 m (4 ft) beam spacingand medium fire. Dark and light grey denotes where a sensor activates before the fire reaches 100 kW and 1.0 MW respectively. White denotes where the sensor would not activate. Activation criteria: when the link temperature rises to $57°C$ $(135°F)$.

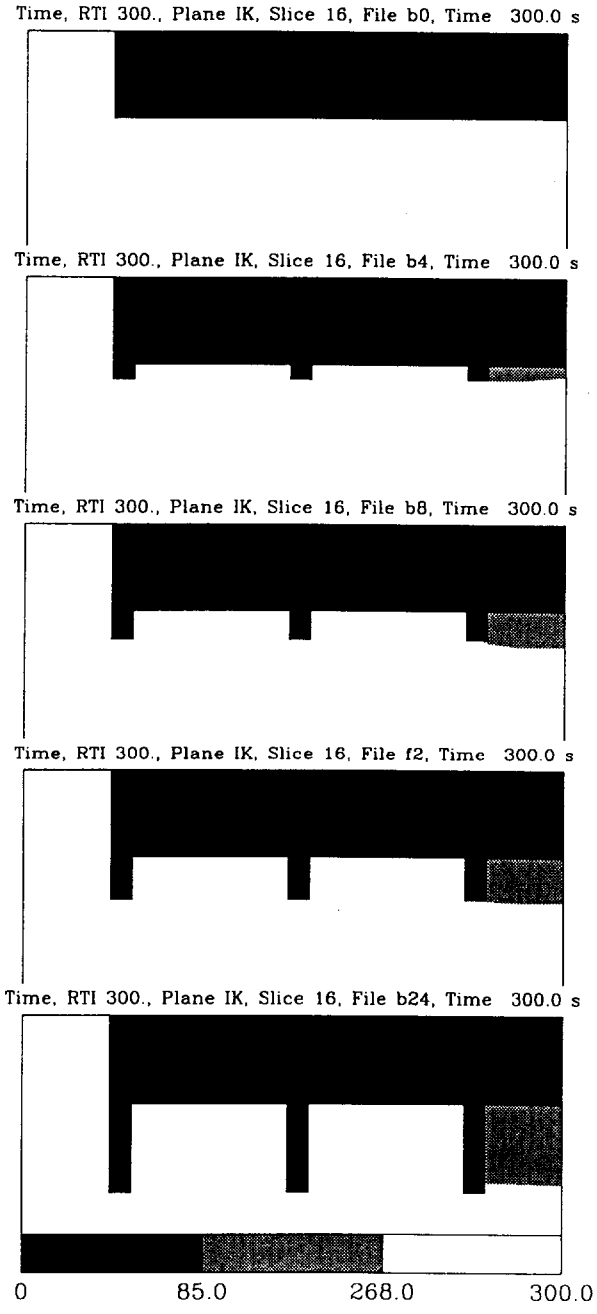

Figure 22: Shaded contour plot of heat detector (RTI = 300) response volumes for various beam depths: 0.0 m (0 in), 0.10 m (4 in), 0.20 m (8 in), 0.30 m (12 in), 0.61 m (24 in)with 3.35 m (11 ft) ceiling height, 1.22 m (4 ft) beam spacingand medium fire. Dark and light grey denotes where a sensor activates before the fire reaches 100 kW and 1.0 MW respectively. White denotes where the sensor would not activate. Activation criteria: when the link temperature rises to $57°C$ ($135°F$).

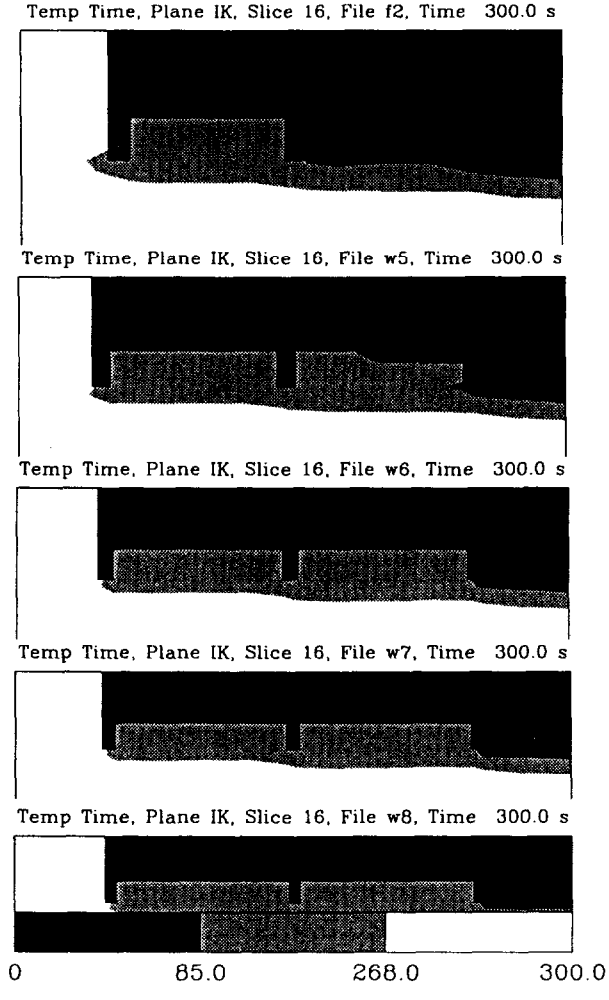

Figure 23: Shaded contour plot of smoke detector response volumes for various on center beam spacings: 1.2 m (4 ft), 1.5 m (5 ft), 1.8 m (6 ft), 2.1 (7 ft), 2.4 m (8 ft)with 0.305 m (12 in) beam depth, 3.35 m (11 ft) ceiling height and medium fire. Dark and light grey denotes where a sensor activates before the fire reaches 100 kW and 1.0 MW respectively. White denotes where the sensor would not activate. Activation criteria: when the gas temperature rises $13°C$ above ambient.

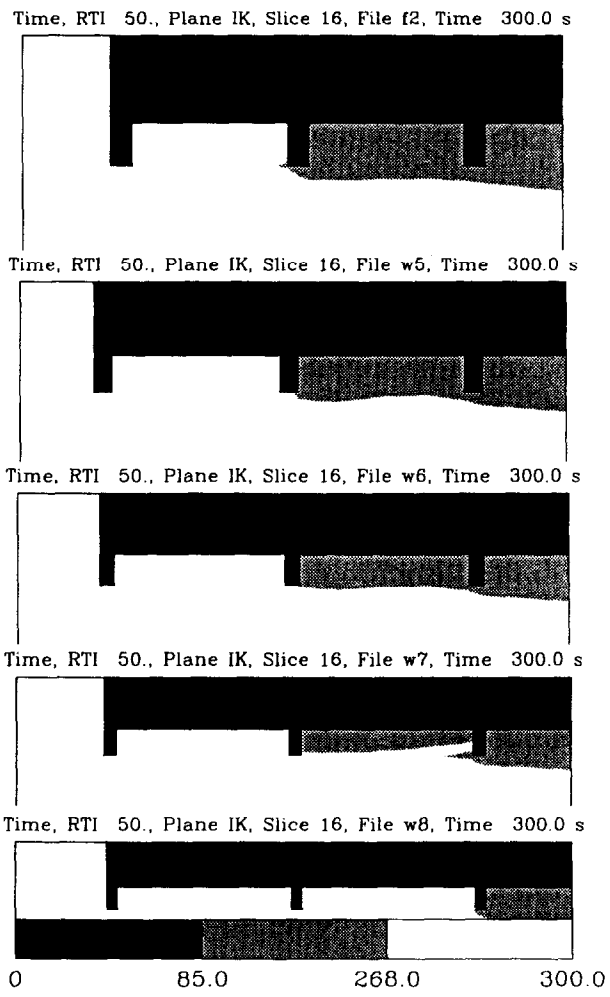

Figure 24: Shaded contour plot of heat detector (RTI = 50) response volumes for various on center beam spacings: 1.2 m (4 ft), 1.5 m (5 ft), 1.8 m (6 ft), 2.1 (7 ft), 2.4 m (8 ft)with 0.305 m (12 in) beam depth, 3.35 m (11 ft) ceiling height and medium fire. Dark and light grey denotes where a sensor activates before the fire reaches 100 kW and 1.0 MW respectively. White denotes where the sensor would not activate. Activation criteria: when the link temperature rises to $57°C$ ($135°F$).

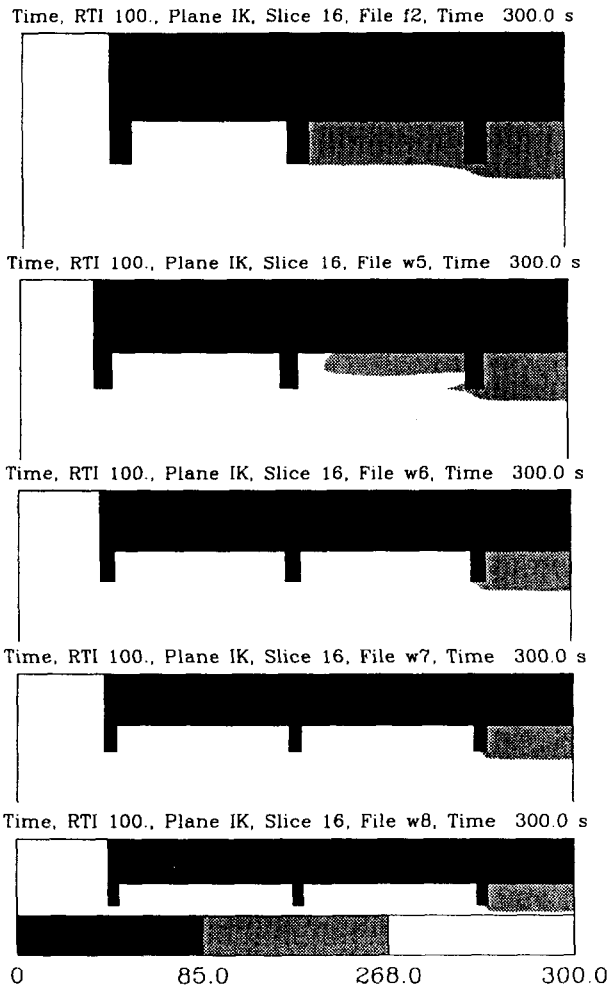

Figure 25: Shaded contour plot of heat detector (RTI = 100) response volumes for various on center beam spacings: 1.2 m (4 ft), 1.5 m (5 ft), 1.8 m (6 ft), 2.1 (7 ft), 2.4 m (8 ft)with 0.305 m (12 in) beam depth, 3.35 m (11 ft) ceiling height and medium fire. Dark and light grey denotes where a sensor activates before the fire reaches 100 kW and 1.0 MW respectively. White denotes where the sensor would not activate. Activation criteria: when the link temperature rises to $57°C$ ($135°F$).

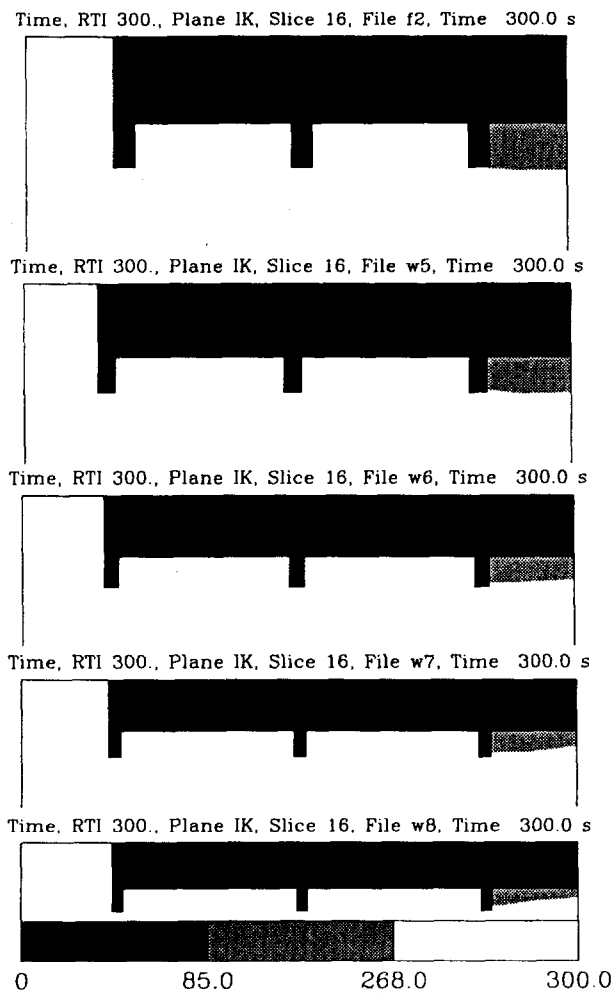

Figure 26: Shaded contour plot of heat detector (RTI = 300) response volumes for various on center beam spacings: 1.2 m (4 ft), 1.5 m (5 ft), 1.8 m (6 ft), 2.1 (7 ft), 2.4 m (8 ft)with 0.305 m (12 in) beam depth, 3.35 m (11 ft) ceiling height and medium fire. Dark and light grey denotes where a sensor activates before the fire reaches 100 kW and 1.0 MW respectively. White denotes where the sensor would not activate. Activation criteria: when the link temperature rises to $57°C$ ($135°F$).

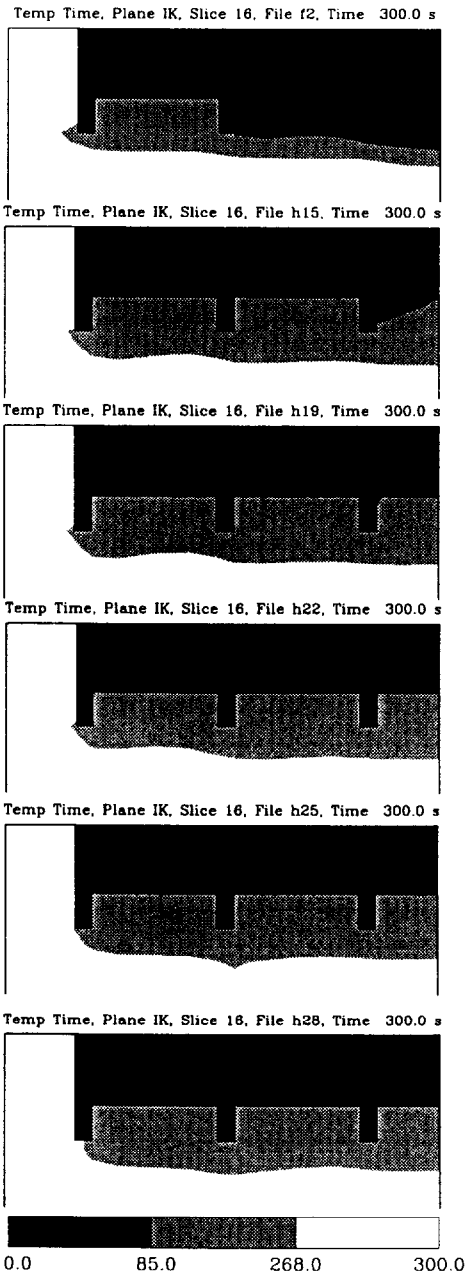

Figure 27: Shaded contour plot of smoke detector response volumes for various ceiling heights: 3.35 m (11 ft), 4.57 m (15 ft), 5.79 m (19 ft), 6.71 (22 ft), 7.62 m (25 ft), 8.53 m (28 ft)with 0.305 m (12 in) beam depth, 1.22 m (4 ft) beam spacing and medium fire. Dark and light grey denotes where a sensor activates before the fire reaches 100 kW and 1.0 MW respectively. White denotes where the sensor would not activate. Activation criteria: when the gas temperature rises $13°C$ above ambient.

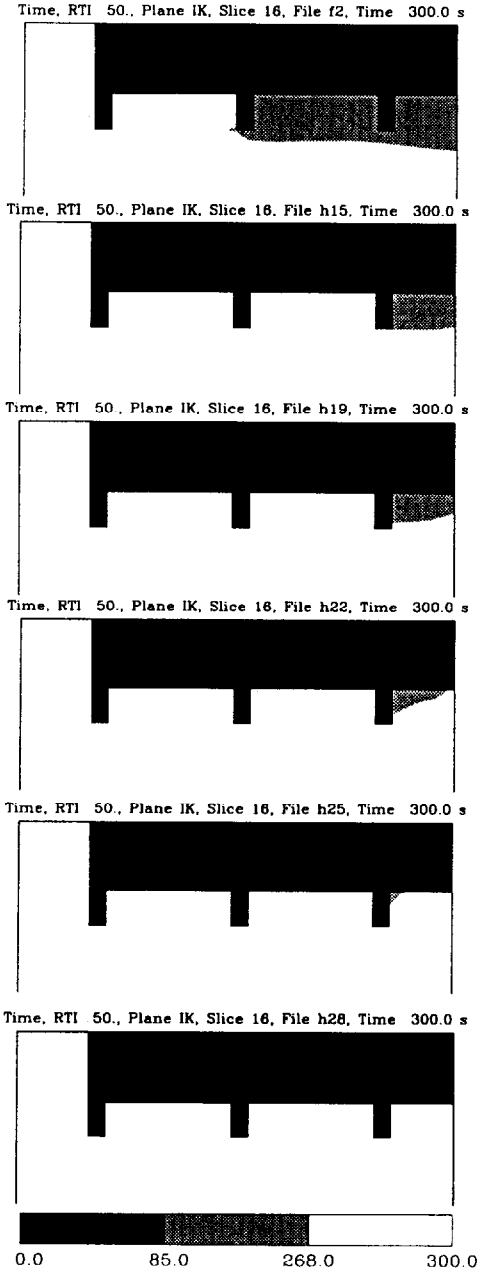

Figure 28: Shaded contour plot of heat detector (RTI = 50) response volumes for various ceiling heights: 3.35 m (11 ft), 4.57 m (15 ft), 5.79 m (19 ft), 6.71 (22 ft), 7.62 m (25 ft), 8.53 m (28 ft)with 0.305 m (12 in) beam depth, 1.22 m (4 ft) beam spacing and medium fire. Dark and light grey denotes where a sensor activates before the fire reaches 100 kW and 1.0 MW respectively. White denotes where the sensor would not activate. Activation criteria: when the link temperature rises to $57°C$ $(135°F)$.

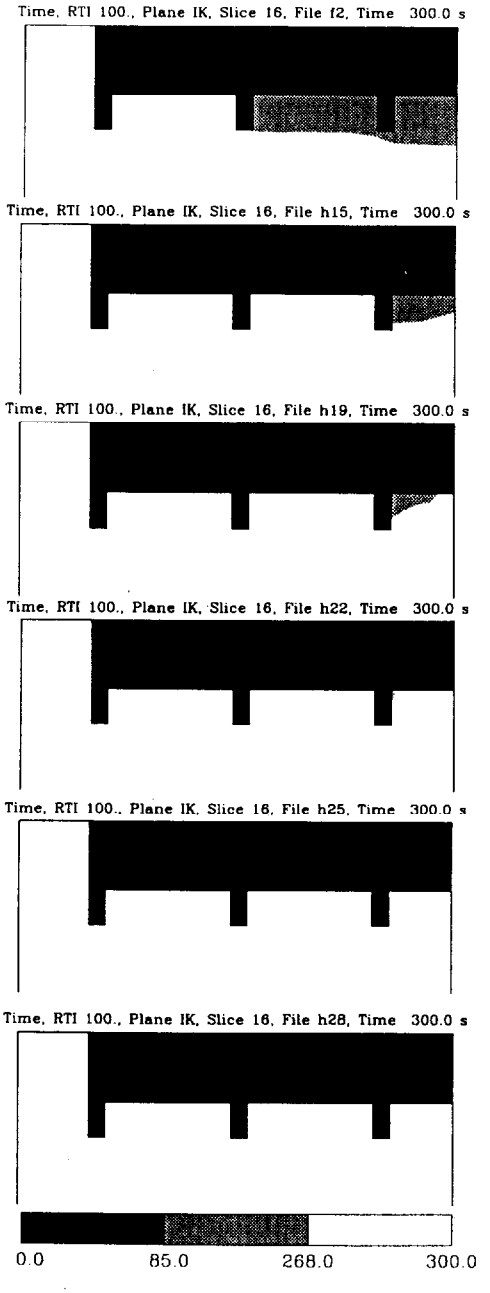

Figure 29: Shaded contour plot of heat detector (RTI = 100) response volumes for various ceiling heights: 3.35 m (11 ft), 4.57 m (15 ft), 5.79 m (19 ft), 6.71 (22 ft), 7.62 m (25 ft), 8.53 m (28 ft)with 0.305 m (12 in) beam depth, 1.22 m (4 ft) beam spacing and medium fire. Dark and light grey denotes where a sensor activates before the fire reaches 100 kW and 1.0 MW respectively. White denotes where the sensor would not activate. Activation criteria: when the link temperature rises to $57°C$ $(135°F)$.

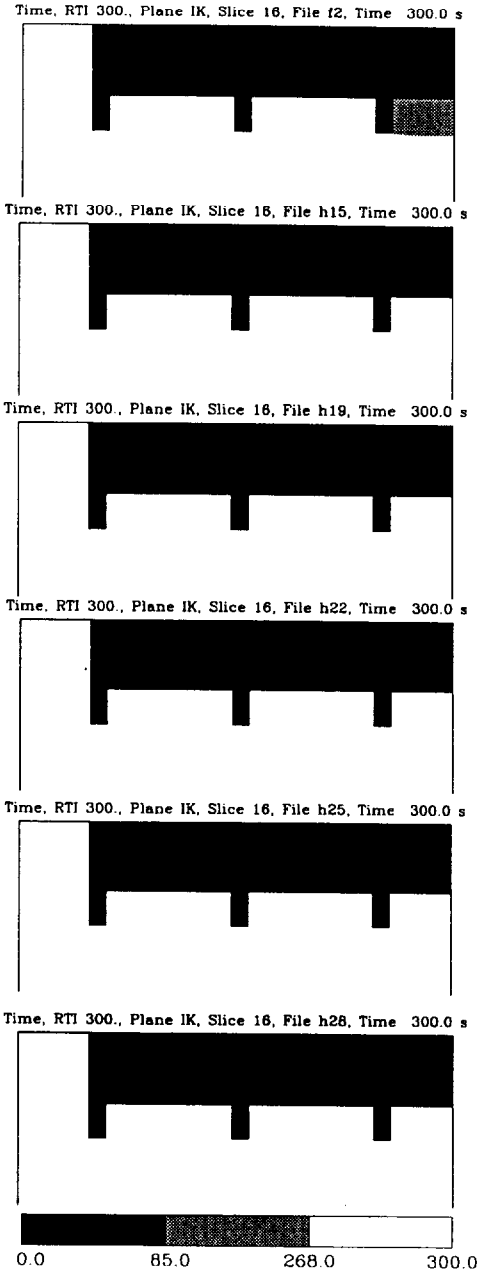

Figure 30: Shaded contour plot of heat detector (RTI = 100) response volumes for various ceiling heights: 3.35 m (11 ft), 4.57 m (15 ft), 5.79 m (19 ft), 6.71 (22 ft), 7.62 m (25 ft), 8.53 m (28 ft)with 0.305 m (12 in) beam depth, 1.22 m (4 ft) beam spacing and medium fire. Dark and light grey denotes where a sensor activates before the fire reaches 100 kW and 1.0 MW respectively. White denotes where the sensor would not activate. Activation criteria: when the link temperature rises to $57°C$ $(135°F)$.

Table 4: Summary of spacing recommendations (bj = under every j'th beam, ci= in every i'th channel) for thermal sensors based on an activation temperature of $57°C$ $(135°F)$ and for smoke detectors based on an activation temperature rise of $13°C$ $(7.2°F)$

Case	Thermal Detector						Smoke Detector	
	RTI = 50		RTI = 100		RTI = 300			
	100 kW	1.0 MW	100 kW	1.0 MW	100 kW	1.0 MW	100 kW	1.0 MW
F1	-	b4/c3	-	b4/c3	-	c1	b2/c3	b6/c5
F2	-	b2/c3	-	b2/c3	-	c1	b2/c3	b6/c5
F3	-	c3	-	c1	-	-	c1	b6/c5
W4	-	b2/c3	-	b2/c3	-	c1	b2/c3	b6/c5
W5	-	b2/c3	-	b2/c1	-	c1	b2/c1	b4/c5
W6	-	b2/c3	-	c1	-	c1	c1	b4/c5
W7	-	b2/c3	-	c1	-	c1	c1	b4/c5
W8	-	c1	-	c1	-	c1	c1	b4/c5
B4	-	b4/c5	-	b4/c5	-	c1	b4/c5	b6/c5
B8	-	b4/c5	-	b4/c3	-	c1	b4/c3	b6/c5
B12	-	b2/c3	-	b2/c3	-	c1	b2/c3	b6/c5
B24	-	c1	-	c1	-	c1	c1	b2/c3
H11	-	b2/c3	-	b2/c3	-	c1	b2/c3	b6/c5
H15	-	c1	-	c1	-	-	c1	b6/c5
H19	-	c1	-	c1	-	-	-	b6/c5
H22	-	c1	-	-	-	-	-	b6/c5
H25	-	-	-	-	-	-	-	b6/c5
H28	-	-	-	-	-	-	-	b4/c5